Characterization of the EcoRecover Process for Intensive Microalgal Cultivation and Tertiary Nutrient Recovery from Wastewaters

Hannah R. Molitor,[1] Ga-Yeong Kim,[1] Elaine Hartnett,[2] Benjamin Gincley,[3] Md Mahbubul Alam,[4] Nickolas M. Avila,[1] Jianan Feng,[1] Autumn Fisher,[2] Mahdi Hodaei,[4] Yalin Li,[5,6] Kevin McGraw,[2] Roland D. Cusick,[1] Ian M. Bradley,[4,7] Ameet J. Pinto,[3] Jeremy S. Guest[1,5,*]

[1] Department of Civil & Environmental Engineering, Newmark Civil Engineering Laboratory, University of Illinois Urbana-Champaign, Urbana, IL, 61801, USA.

[2] Clearas Water Recovery, Inc., Missoula, MT 59808, USA.

[3] School of Civil and Environmental Engineering, Georgia Institute of Technology, Atlanta, GA 30332, USA.

[4] Department of Civil, Structural and Environmental Engineering, University at Buffalo, The State University of New York, Buffalo, NY 14260, USA.

[5] Institute for Sustainability, Energy, and Environment, University of Illinois Urbana-Champaign, Urbana, IL 61801, USA.

[6] Department of Civil and Environmental Engineering, Rutgers, The State University of New Jersey, Piscataway, NJ 08854, USA.

[7] Research and Education in Energy, Environmental and Water (RENEW) Institute, University at Buffalo, The State University of New York, Buffalo, NY 14260, USA.

*Corresponding author: jsguest@illinois.edu, +1 (217) 244-9247

Keywords (5–8 keywords)**:** photobioreactors; membrane bioreactor; nutrient recovery; circular bioeconomy; microalgal-bacterial community; microalgae; biopolymer

Abstract

Mixed community microalgal wastewater treatment technologies have the potential to advance the limit of technology for biological nutrient recovery while producing a renewable carbon feedstock, but a deeper understanding of their performance is required for system optimization and control. In Fall 2020, a 568 $m^3 \cdot day^{-1}$ (150,000 $gal \cdot day^{-1}$) Clearas EcoRecover microalgal treatment system was installed at the Village of Roberts (Wisconsin, USA; latitude 45.0°N) wastewater treatment plant to meet their pending effluent permit of 0.04 $mg \cdot L^{-1}$ total phosphorus (TP; 6-month average). Here we report data and analyses from continuous on-line system monitoring, long-term on-site monitoring, and on-site batch experiments, with particular focus on a 3.5 month winter period with limited outside influences (e.g., no major upstream process changes). Across this period of intensive monitoring, effluent TP concentrations were consistently below 0.03 $mg\text{-}P \cdot L^{-1}$ for 3 months. Core microbial community taxa included *Chlorella spp.*, *Scenedesmus spp.*, and *Monoraphidium spp.*, and key indicators of stable performance included near-neutral pH, sufficient alkalinity, and a diel rhythm in dissolved oxygen. By tracking elemental and biochemical composition of the biomass, we also demonstrated the importance of carbohydrate storage (in photobioreactors) and mobilization (in a dark mix tank) in achieving reliable nutrient recovery and algal growth.

Synopsis Statement

This study characterizes the performance of the first full-scale installation of the EcoRecover mixed community microalgal wastewater treatment process.

TOC Graphic

1. Introduction

The United States Environmental Protection Agency estimates that nutrients impair 15-41% of assessed surface water area (including lakes, rivers, estuaries, etc.) in the United States.[1] Phosphorus, specifically, is the limiting nutrient for harmful algal growth and eutrophication in many freshwater ecosystems.[2] To protect or restore US waters, states are adopting numeric water quality criteria for nitrogen and phosphorus by identifying impaired water bodies and adjusting effluent permits for water resource recovery facility (WRRF) to meet waterbody-specific loadings.[3] As of 2021, eight states had gained state-wide phosphorus criteria for at least one waterbody type, while another sixteen states had added numeric criteria for select waterbodies (headwaters, wadeable streams, reservoirs requiring algicide, etc.).[4] To meet increasingly prevalent and increasingly stringent effluent phosphorus limits to protect natural waterbodies, wastewater treatment plants are in need of effective and cost-efficient technologies that reliably achieve phosphorus removal or recovery.

To date, commercialized tertiary wastewater treatment technologies for phosphorus management have been limited to enhanced biological phosphorus removal (EBPR), chemical polishing, and membranes.[5] EBPR can be a lower cost among these options but cannot reliably treat below 0.3 $mg \cdot L^{-1}$ total phosphorus.[6] Though chemical polishing with coagulants (typically

aluminum sulfate or ferric chloride) can achieve more stringent effluent limits, significant addition of these chemicals generates large quantities of sludge that are difficult to treat, are expensive to landfill, and that represent a recalcitrant precipitate that make phosphorus recovery challenging.[7] Additionally, reliably achieving very low phosphorus effluent concentrations (e.g., <0.1 mg-P·L^{-1})[8] requires coagulant dosing that is significantly higher than predicted by stoichiometric quantities due to numerous side reactions, and the stoichiometric disparity increases substantially as target effluent phosphorus concentrations decrease.[9] Once precipitated, phosphorus-recovery from chemical polishing sludge requires chemical extraction and/or thermal approaches at very high temperatures (1,000 to 2,000 °C).[10] As an alternative to bacteria-driven luxury uptake in EBPR and to chemical polishing, microalgae can achieve phosphorus recovery – including organic phosphorus that is otherwise recalcitrant in conventional WRRFs[11,12] – through assimilation into (i.e. recovered as) biomass. If algal treatment systems can be engineered to reliably meet effluent nutrient permits, they have the potential to leverage waste phosphorus for CO_2 fixation and the production of renewable bioproducts and biofuels in support of a circular economy.[13]

The EcoRecover process is an intensive (i.e., high areal productivity, small footprint) tertiary nutrient recovery process which leverages the Advanced Biological Nutrient Recovery (ABNR™, Clearas Water Recovery Inc.)[14] system. The process consists of a dark mix tank, photobioreactors (PBRs), and the separation of the hydraulic retention time (HRT) and solids residence time (SRT) with membranes (**Figure 1**). The EcoRecover ABNR process was first piloted as a batch system, with minimal monitoring, at the South Davis Sanitary District (South Davis, Utah, USA) beginning in August 2016. In Fall 2021, the first full-scale installation began operation at the Village of Roberts (Wisconsin, USA), with robust monitoring and a design flow of 568 m^3·day^{-1}. As of Fall 2023, a 1,100 m^3·day^{-1} EcoRecover system has been constructed in Mondovi (Wisconsin, USA) and a 10,600 m^3·day^{-1} system is operating in Waupun (Wisconsin, USA). To date, however, there is no publicly available data on the performance of the EcoRecover

process or documentation of its full-scale performance. Broad adoption of intensive (i.e., high productivity, small footprint) microalgal treatment technologies requires data transparency and an understanding of factors governing process performance to enable mechanistic system design and control.

The objective of this work was to characterize the full-scale performance of the EcoRecover system as a tertiary treatment process for phosphorus removal and recovery from wastewater. The EcoRecover system was deployed as a tertiary treatment process to achieve effluent total phosphorus concentrations below new water quality-based permit limits of 0.12 mg-P·L^{-1} (monthly) and 0.04 mg-P·L^{-1} (6-month average) for the full forward (design) flow of 568 m^3·day^{-1} (150,000 gal·day^{-1}). Continuous, long-term monitoring was achieved through a network of sensors and analyzers that interfaced with a supervisory control and data acquisition system (SCADA) and were complemented by alternate-day elemental analysis of the solids and twice daily aqueous and total suspended solids (TSS) analyses during weekdays. These long-term monitoring data were supplemented with batch kinetic assays to better understand drivers of performance. Periods with effluent total phosphorus concentrations below the discharge limit were observed, stable performance indicators were identified, and carbon and nutrient dynamics within and across unit operations were characterized. Ultimately, a deeper understanding of the EcoRecover system will support further system optimization and control to advance the sustainability of microalgal wastewater treatment technologies and biological nutrient recovery.

2. Materials and Methods

2.1. Full-scale Treatment System and Long-Term Operation

The Roberts Wastewater Treatment Plant (WWTP; Village of Roberts, WI, USA) has an average influent flow of 410 m^3·day^{-1} and a design flow of 568 m^3·day^{-1} for a municipality of nearly 2,000 residents.[15] The Wisconsin Department of Natural Resources decreased the Roberts WWTP's

Wisconsin Pollutant Discharge Elimination System's (WPDES No. 0028835) 6-month average effluent phosphorus limit from 1 mg-P·L^{-1} to 0.04 mg-P·L^{-1}, effective February 1, 2021, to protect and recover the water quality of the effluent receiving bodies, the East and West Twin Lakes.[16] The EcoRecover process, which the Village elected to implement for phosphorus-removal, was constructed in 2020 and 2021 (**Figure 1**, SI Figure S1). Secondary effluent from sequencing batch reactors (SBRs) is mixed with the microalgal community in a mix tank (average working volume of 98 m^3 gal) before being sparged with CO_2 and pumped through five parallel sets of PBRs (77.6 m^3 total). The PBRs are housed in a greenhouse and, in addition to daylight, receive an average of 100 μmol ·m^{-2}·s^{-1} photons from supplemental lighting from 54 LEDs (California Light Works MegaDrive™ Centralized Power LED Network). The separation of HRT and SRT is achieved via submerged, hollow fiber ultrafiltration modules in two parallel membrane tanks with average transmembrane pressure of 15.4 kPa (Puron ultrafiltration hollow fiber submerged membrane module, Model PHF960, 3.8 m^3 working volume per train, 18 rows per module, 0.03 μm pores, Koch Separation Solutions, Inc.). A fraction of the permeate is stored in an 11.4-m^3 reuse tank (averaged measured HRT of <10 min) for membrane backwashing while the remainder is discharged as effluent. Harvested solids are pumped from the membrane tank and dewatered via centrifugation (Disk Stack Clarifier AC1200-410, Flottweg Separation Technology, Independence, KT, USA). Centrate is mixed in a return tank (6.4 m^3; averaged measured HRT of 20 min) with the PBR recycle flow and retentate from the membrane tanks before the combined flow returns to the mix tank.

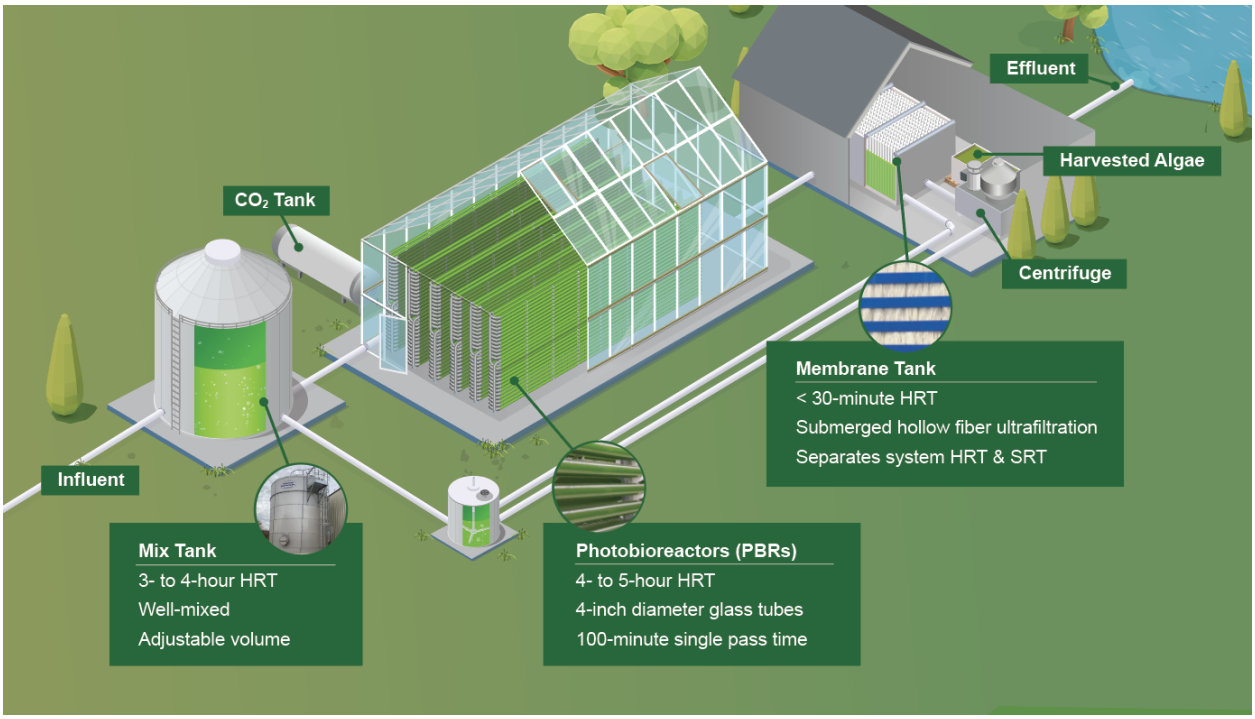

Figure 1. EcoRecover process flow diagram. The mix tank receives secondary effluent and recycled microalgal biomass under dark, nutrient-replete conditions. Inorganic carbon is sparged into the mixed microbial community just prior to the PBRs where the biomass receives light, and conditions become phosphorus-limited. Ultrafiltration in the membrane tank (membrane bioreactor) separates the tertiary effluent from the biomass, which is either recycled back to the mix tank or harvested.

The mix tank, a nutrient-replete, dark environment, operates as a completely stirred tank reactor, is well-mixed through intermittent sparged aeration with resulting dissolved oxygen generally below 5 $mg \cdot L^{-1}$. Mix tank effluent flows to the PBRs, where the microalgal community is exposed to light, a nutrient-deplete environment, and a single-pass time of 100 min. The median measured hydraulic retention times (HRTs) of the mix tank and PBRs are 3.3 and 4.3 hrs, respectively. Batch, bench-scale kinetic experiments were conducted for durations that exceeded

146 the single pass times of the full-scale unit processes to better characterize the kinetics and
147 stoichiometry of nutrient uptake and carbon storage and mobilization.

148 For this study we focused on monitoring data from November 1, 2022 to February 14,
149 2023, which represented an extensively sampled period with limited outside influences (e.g., no
150 upstream plant changes, no known chemical perturbation events). Examples of periods with
151 significant outside influence are presented in Section 3.1.3. and SI Section S6 for transparency
152 but are not the focus of this study.

153 **2.2. Bench-Scale Batch Experiments**

154 Bench-scale, batch experiments were conducted to characterize carbon and nutrient dynamics in
155 the full-scale mix tank and PBRs. Duplicate batch experiments were conducted in cylindrical,
156 bench-scale PBRs constructed from clear cast acrylic with the same diameter as the full-scale
157 system (102 mm i.d., 91 cm height, 7 L working volume). The bench-scale PBRs were placed in
158 the greenhouse with the full-scale PBRs to match light and temperature conditions. A third PBR
159 (102 mm i.d., 69 cm height, 5 L working volume) was run in parallel, without being sampled, to
160 ensure sufficient solids for the subsequent mix tank bench-scale experiment. Bench-scale mix
161 tank experiments were conducted in duplicate under dark conditions in opaque, HDPE plastic
162 containers (4-L working volume) with lids.

163 Bench-scale experiments were inoculated with biomass and process flows taken directly
164 from the full-scale system immediately before initiation of the batch experiments. The bench-scale
165 PBR experiments were conducted using effluent from the full-scale mix tank (20 L). To ensure
166 the biomass in the mix tank batch experiments had adequate stored carbon (at the start of the
167 experiment) to observe organic carbon mobilization, the mix tank experiments were conducted
168 using secondary effluent combined with the biomass from the bench-scale PBR that was not
169 sampled (2.2 L and 5.8 L, respectively, to match the mixing ratio in the full-scale mix tank).

Reactors were continuously mixed (magnetic stirrer; 300 rpm) and sampled with wide-bore 50 mL serological pipets at 0, 10, 20, 40, 60, 90, 120, 150, 180, and 240 min (PBRs were also sampled at 300 min and 360 min). The aqueous fraction of samples was immediately separated from the solids through centrifugation at 4,200 x g for 5 min at 4 °C (5804R Eppendorf centrifuge; Enfield, CT, USA) and then filtered through 0.22 µm (MF-Millipore™ Membrane Filter, 0.22 µm, item no. GSWP02500; MilliporeSigma). The solids pellet and filtered aqueous samples were stored separately at -20 °C prior to lyophilization (solids samples) and analysis (solids and aqueous samples). TSS and volatile suspended solids (VSS) were quantified at 0, 120, and 240 min (as well as 360 min for the PBRs). The reactor pH was maintained between 6.8 and 7.5 to avoid pH inhibition; adjustments were accomplished with 2 M HCl. The alkalinity of PBR samples – determined via titration of 100 mL samples to pH 4.5 (Mettler Toledo DL55 titrator) – was initially 600 $mg \cdot L^{-1}$ as $CaCO_3$ and maintained above 200 $mg \cdot L^{-1}$ as $CaCO_3$ through $NaHCO_3$ addition to avoid carbon limitation.

2.3. Continuous On-Line Monitoring

For the continuously operating full-scale system, long-term monitoring was achieved through online sensors and analyzers for pH, dissolved oxygen (DO), TSS, PO_4^{3-}, NH_4^+, NO_3^-, turbidity, temperature, and photosynthetically active radiation (PAR; Table S1 and Figure S2 in the SI), which interfaced with a SCADA system. Hydraulic parameters, including flowrates and tank volumes, were also collected through on-line monitoring. Most sensors were on-line by late November 2020. Following the International Water Association Good Modeling Practice Unified Protocol,[17] the long-term continuous online monitoring data were reconciled to ensure that systematic errors (e.g., shifts or drifts) in the data set were identified and resolved using the kernel smoothing method of a Python package for functional data analysis (scikit-fda).[18] In particular, pH, TSS, PO_4^{3-}, NH_4^+, and NO_3^- were additionally corrected to match the magnitude of the daily

194 onsite laboratory measurement data (SI_SCADA and SI_AIMS spreadsheets, Supporting
195 Information, SI).[19]

196 **2.4. Aqueous and Suspended Solids Analyses**

197 **2.4.1. Long-Term On-Site Monitoring**

198 Beginning in December 2021, long-term continuous on-line monitoring was supplemented by
199 analyses of once to twice daily grab and 24-hour composite samples from the full-scale system.
200 Aqueous parameters were measured with Hach kits after samples were filtered through 0.45 µm
201 mixed cellulose ester filters. Specifically, aqueous samples were analyzed for orthophosphate
202 and total phosphate (Hach TNT843); alkalinity (TNT870); nitrate (TNT835 or TNT836; dependent
203 on sample concentration range); ammonium (TNT830, TNT831, or TNT832; dependent on
204 sample concentration range); nitrite (TNT839 and TNT840); and total nitrogen (TNT827). The
205 method detection limit (MDL) and minimum reporting level (MRL) for total phosphorus and
206 orthophosphate were estimated according to Ripp 1996,[20] and were, respectively, found to be
207 0.005 and 0.005 mg-P·L^{-1} (MDL) and 0.014 and 0.016 mg-P·L^{-1} (MRL; SI Table S2). Briefly, 9
208 replicates of the same concentration were analyzed using TNT843, and MDL was defined as the
209 product of the t-value for n-1 samples (t = 2.896) and the sample standard deviation of those
210 replicates. MRL was defined as three times the value of the MDL.

211 **2.4.2. Batch, Bench-Scale Analyses**

212 Batch experiment samples (solids and aqueous) were analyzed both on-site and at the University
213 of Illinois Urbana-Champaign (UIUC). Handheld probes were used to measure pH (Orion 3-Star
214 portable pH meter; Thermo Scientific), temperature and DO (Orion RDO dissolved oxygen probe;
215 Thermo Scientific), and ammonium concentrations (ProDSS multiparameter digital water quality
216 meter; YSI); each sensor was calibrated immediately prior to use in the bench-scale experiments.
217 Solids storage and analyses for TSS and VSS were performed as in Bradley et al. 2021.[21–25]

Briefly, sample TSS was determined by filtration though 0.7 μm glass fiber filters (Whatman GF/F). After filtration, filters were heated at 105 °C for 1 h and desiccated for 30 min prior to weighing. VSS was determined by combusting samples for 20 min at 550 °C.

Samples for phosphate, nitrate, and nitrite were immediately filtered with 0.22 μm filters and frozen. After storage, aqueous samples were thawed and re-filtered prior to analysis via ion chromatography (Dionex ICS-2100 ion chromatograph, Dionex IonPac AS18 column; SI Section S2 Figures S3-S5 for calibration curves). The average MRL for phosphate was determined to be 0.027 mg-P·L^{-1} and the MRL range was 0.022 to 0.037 mg-P·L^{-1} (SI Section S2, Table S3).

2.5. Solids Characterization

2.5.1. Elemental Composition

For the elemental analysis of biomass, a solids pellet was collected through centrifugation of a culture sample, immediately frozen, and then lyophilized for 48 hrs. Phosphorus content was measured through inductively coupled plasma mass spectrometry (ICP-MS; Model NexION 350D, PerkinElmer) and elemental carbon, nitrogen, and hydrogen were measured with a CHN Analyzer (Model CE440, Exeter Analytical) by the UIUC Microanalysis Laboratory. If replicate results had a greater than 5% difference, the sample was reanalyzed and the results were replaced.

2.5.2. SEM-EDS Biomass Surface Characterization

The surface of lyophilized and ground solids samples were characterized using Scanning Electron Microscopy-Energy Dispersive Spectroscopy (SEM-EDS)[26–28] in the Microscopy Suite at the Beckman Institute for Advanced Science and Technology at UIUC. Before imaging, the samples were mounted on a stub using carbon tape. The samples were imaged using a SEM (Model Quanta FEG 450, FEI company) operating at 15.0 kV under the low vacuum mode and at a working distance of 10 mm. The elemental compositions were measured using the EDAX light-element energy-dispersive spectroscopy system (AMETEK, Inc.) attached to the SEM.

2.5.3. Carbohydrate, Protein, and Lipid Quantification

Solids storage and analyses for protein-to-N ratio and carbohydrate content were performed as in Bradley et al. 2021.[21–25] Briefly, protein content was estimated by multiplying the elemental nitrogen content by a conversion factor that represents the ratio of N content to protein. Conversion factors were determined by analysis of amino acid residuals; amino acid profiling was performed by Bio-Synthesis, Inc. (Lewisville, Texas, USA). Total monomeric carbohydrate content of lyophilized solids was determined after a two-step acid hydrolysis of the complete biomass. The hydrolysate was neutralized, filtered, and the monosaccharide concentration was quantified against glucose standards. Solids crude lipid content was quantified as in Gardner-Dale et al.[24,29,30] Briefly, crude lipids from lyophilized solids were extracted using an adaptation of the Folch method and a 2:1 (v/v) chloroform:methanol solvent mixture. After the extraction, sodium chloride solution was added to bring the final mixture to a 8:4:3 ratio of chloroform:methanol:sodium chloride. The mixture was centrifuged, resulting in a biphasic system; the bottom phase containing the crude lipids was transferred to weighting dishes to be measured gravimetrically after the carrier solvent evaporated.

2.5.4. Flow Imaging Microscopy

Mix tank effluent samples (10 mL in a 15 mL conical tube) were collected once daily. Samples were diluted to approximately $1x10^6$ particles per milliliter prior to running on a FlowCam 5000 flow imaging microscope (Yokogawa Fluid Imaging Technologies, Inc.). The resulting collection of detected particles was screened to remove background objects, then used as input data fora deep learning classification model trained on representative libraries of the dominant taxonomic groups observed in the system. Details are in SI Section S5.

2.5.5. High Throughput 18S rRNA Sequencing

1-mL samples of suspended biomass from the mix tank and PBR effluent were collected in triplicate and stored in 5-mL polypropylene transport tubes filled with 3 mL Zymo DNA/RNA Shield. Samples were kept at -20°C until they were shipped overnight on ice to the University at Buffalo (UB) SUNY. DNA extraction was performed using the DNeasy Powersoil Pro Kit (Qiagen), and extracts were stored at -20°C. PCR amplification of the eukaryotic 18S rRNA genes targeted the V8-V9 region (details in Bradley et al., 2016).[31] Gel electrophoresis was conducted post PCR, and bands of expected size and quality were purified using the QIAquick gel purification kit (Qiagen). The purified amplicons from each sample were pooled into a DNA library at equimolar proportions (10 ng). Sequencing was performed on the Illumina MiSeq platform with v3 chemistry (300-cycle paired-end reads) at the UB Genomics and Bioinformatics Core. Raw sequencing data are available on NCBI under BioProject accession number PRJNA1045645. The sequencing read processing (i.e., quality filtering and trimming, taxonomic assignment) and statistical analyses (including alpha and beta diversity) were conducted following the established protocol (MiSeq SOP) provided by mothur v1.48.0.[32]

3. Results and Discussion

3.1. Characterization of Long-Term Performance

3.1.1. Achieving Non-Detect Effluent Phosphorus and Identifying Key Indicators of Stable System Performance

The first full-scale installation of the EcoRecover process at Roberts, Wisconsin has demonstrated phosphorus recovery from secondary effluent via microalgal biomass cultivation 24-hours per day and across seasons. Periods of performance with effluent total phosphorus concentrations below the discharge limit (<0.04 mg-P·L^{-1}) were observed for sustained periods (months at a time), frequently reaching non-detect values.

The focus period (November 1, 2022 through February 14, 2023; 106 days) began with a two week upset and recovery period, followed by 92 days (November 15, 2022 through February 14, 2023) of superior performance in which the system continuously achieved effluent (permeate) orthophosphate concentrations below 0.04 mg-P·L^{-1} (**Figure 2**, SI Figure S6). Across the full focus period, the effluent total phosphorus concentration of 24-hour composite samples averaged 0.06 ± 0.11 mg-P·L^{-1} (0.03 ± 0.08 mg-P·L^{-1} orthophosphate; average ± standard deviation); within the 92-day period of excellent performance, the effluent total phosphorus concentration averaged 0.03 ± 0.03 mg-P·L^{-1} (0.01 ± 0.02 mg-P·L^{-1} orthophosphate). Effluent ammonia concentrations were highly variable (Figure S7); some nitrification and minimal nitrite concentrations were observed from November 1 to December 8, 2022. (SI Figures S8 and S9). From December 8, 2022 to February 14, 2023, nitrification was negligible.

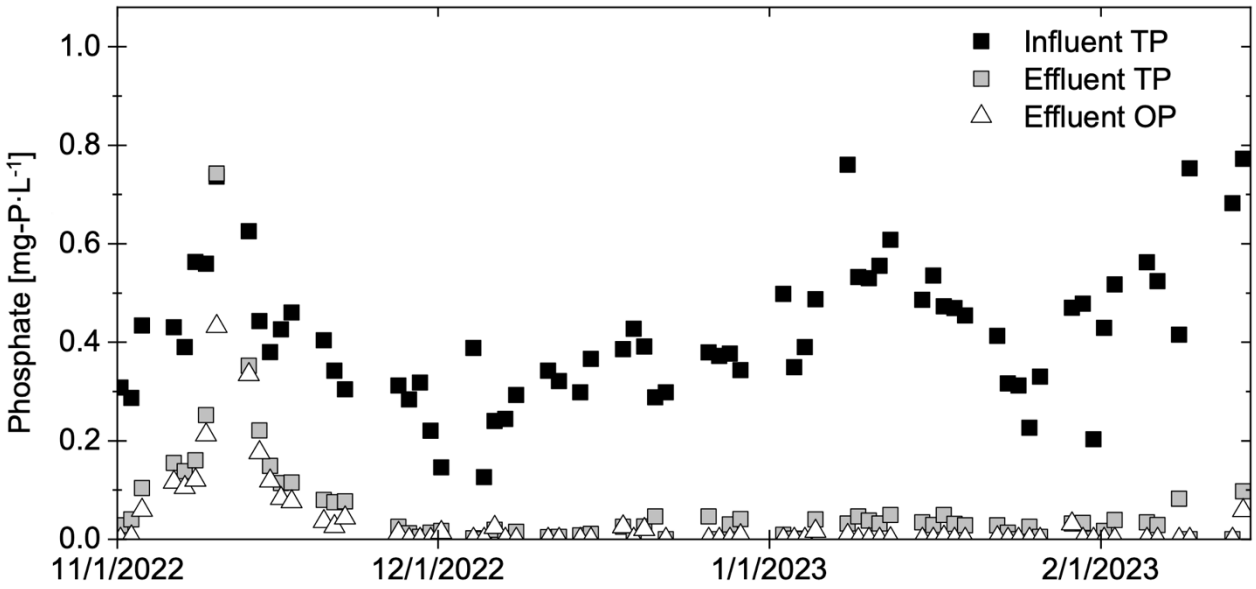

Figure 2. Influent and permeate total phosphorus (TP) concentrations and permeate orthophosphate (PO_4^{3-}) concentrations for the EcoRecover process in winter from November 1, 2022, to February 14, 2023. 24-hour composite samples were collected and immediately analyzed by an on-site laboratory technician (EH).

Across the entire focus period, the algal community was relatively stable. Flow imaging microscopy identified *Chlorella spp.*, *Scenedesmus spp.*, and *Monoraphidium spp*. as dominant constituents of the microalgal community (**Figure 3A-E**). High-throughput sequencing of 18S rRNA genes confirmed the eukaryotic community was dominated by green microalgae, including *Scenedesmus* (28% – 63%), *Desmodesmus* (5% – 31%), and *Chlorella* (0.5% – 26.5%; **Figure 3F**). The eukaryotic community remained stable during this period (**Figures 3G**), as indicated by a consistent Bray-Curtis dissimilarity among samples across the intensive sampling period from the starting community on November 2, 2022 (mean = 0.42, std. dev. = 0.06, and coeff. of variation = 0.14; **Figure 3G**). Additionally, when compared to a variable performance period (February 15, 2023 to April 28, 2023) immediately following the focus period, eukaryotic communities in these two periods showed significantly different clusters ($p < 0.01$, AMOVA)[33] as illustrated by ellipses encompassing 95% of cluster assigned datapoints (SI Figure S10). Full, longer-term sequencing results and more in-depth community structure analyses are the focus of a separate study.

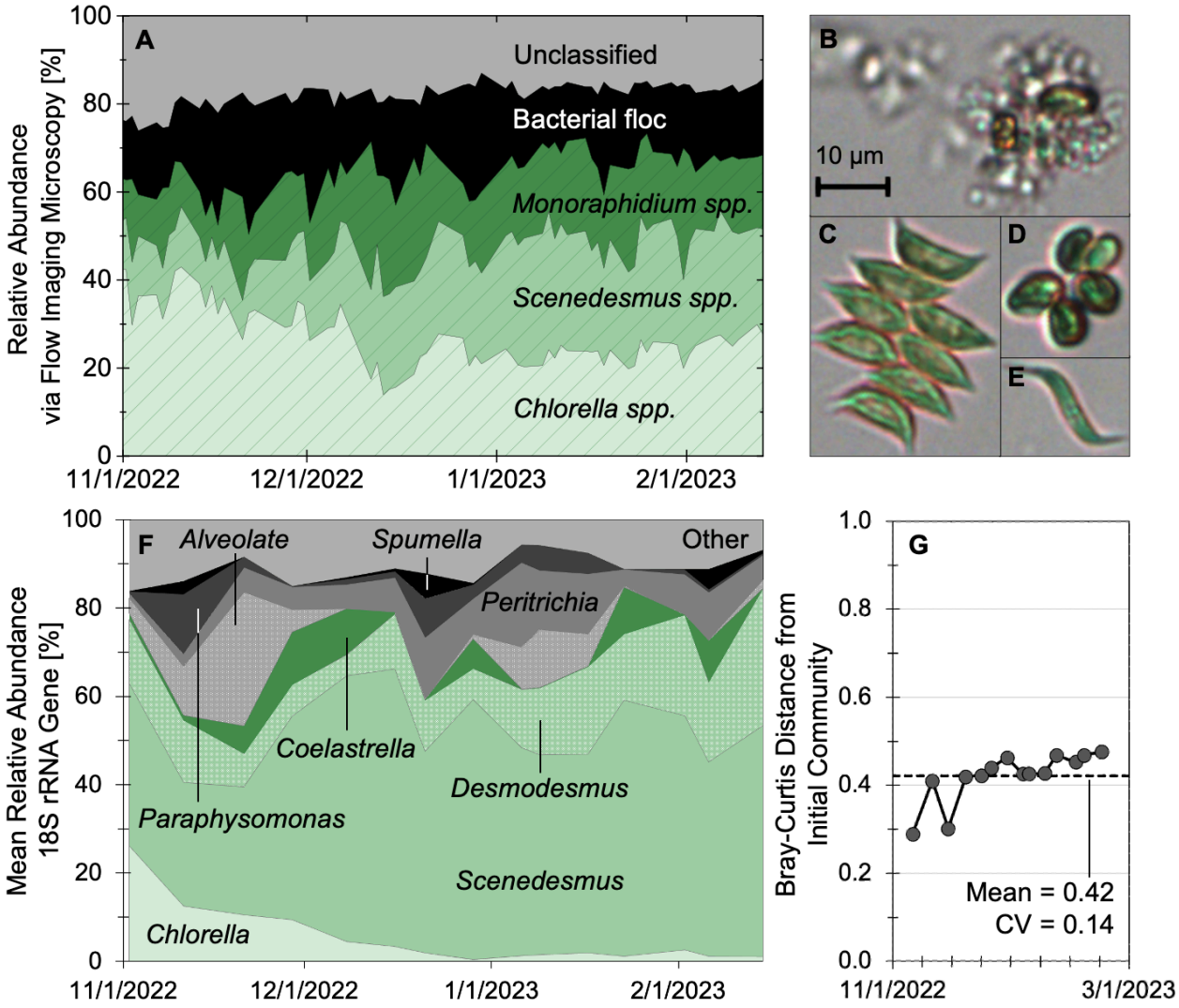

Figure 3. (**A**) Mixed microbial community taxa distribution for the EcoRecover process from November 1, 2022 through February 14, 2023. (**B-E**) FlowCam images of the four dominant categories identified via flow imaging microscopy during this period: (**B**) bacterial floc; (**C**) *Scenedesmus spp.*; (**D**) *Chlorella spp.*; and (**E**) *Monoraphidium spp.* (**F**) Mean relative abundance (MRA) of the top eukaryotic genera from 18S rRNA sequencing. (**G**) Bray-Curtis distances of each sampling point from the initial eukaryotic community on November 2, 2022.

Key indicators of stable performance included near-neutral pH throughout the system, sufficient alkalinity in the EcoRecover influent (>200 $mg \cdot L^{-1}$ as $CaCO_3$) and residual alkalinity in

the EcoRecover effluent (>100 $mg \cdot L^{-1}$ as $CaCO_3$), and a steady daily rhythm in the DO concentration of both the mix tank effluent and PBR effluent (Figure S11). In particular, the cycling of DO concentration in the PBRs is readily apparent (often reaching 10-20 $mg \cdot L^{-1}$), corresponds to the photosynthetic activity of the microalgal community, and generally follows the rhythm of natural light intensity (SI Figure S12).

3.1.2 Solids Composition and Yield

Across the full focus period, the average biomass yield was 33 ± 8 kg $TSS \cdot (kg\text{-}P)^{-1}$, corresponding to a phosphorus content of 3.2 ± 0.7% ($5^{th}/50^{th}/95^{th}$ percentiles of 1.92%/3.56%/4.40%; n = 32) in harvested biomass (SI Figure S13). The phosphorus content in algal biomass has been shown to vary across species[34,35] and also within species as a function of their physiological state.[36–40] The phosphorus content in microalgal cells is often around 1% of dry weight under limited phosphorus availability[41] but may be as high as 4-6% dry weight, inclusive of microalgae achieving luxury uptake of phosphorus.[42–44] Given that the phosphorus content of the harvested biomass is inversely proportional to the total mass harvested and revenue from biomass sales, harvested biomass was further analyzed to better understand the distribution of phosphorus in the solids.

Elevated phosphorus in the biomass may have resulted from both luxury uptake and precipitation within EPS. SEM-EDS was performed on a range of samples from across the entire monitoring period (April 5, 2022 to February 13, 2023; SI Section S4.2 Table S5), including samples with the highest and lowest phosphorus content, from periods with and without coagulant use, and start and end points of batch experiments. Of selected samples for SEM-EDS imaging, the February 13, 2023, sample had the greatest overall phosphorus content (5.08%). Phosphorus-rich granules were observed in biomass samples and appear to be closely associated with the microalgal cells, indicating that elevated phosphorus could be due to precipitation of inorganic phosphorus with metals in extracellular polymeric substances (EPS), as is commonly observed in EBPR biomass (Figure S13).[26,28] Since the dominant taxa at this date

was *Scenedesmus spp.* (**Figure 3**) – which is capable of polyphosphate accumulation – it is possible the granules were associated with luxury update and release, which can induce precipitation within EPS.[38] High pH at the surface of microalgal cells is also expected due to inorganic carbon fixation, which may have facilitated inorganic phosphorus precipitation on the cell surfaces or within cell EPS even at low total phosphorus concentrations.[45–47] Beginning in December 2021, alum (aluminum sulfate liquid #41817; Hawkins, Inc.; Roseville, Minnesota) or Aqua Hawk® 15047 (an inorganic coagulant/polymerized aluminum chlorosulfate solution; Hawkins, Inc.; Roseville, Minnesota) were frequently used at the headworks of the Roberts WWTP to manage influent quaternary ammonium (pandemic disinfectant and microalgal inhibitor) and to attenuate excess influent phosphorus concentrations (i.e., concentrations >0.6 mg-P·L^{-1}). During periods of coagulant use, which frequently corresponded to the highest bulk solids phosphorus content, the imaged solids had elevated metal content (Al, Ca, Mg) and granules of localized elevated phosphorus and metals (SI Figure S14). In periods without coagulant use, inorganic phosphorus granules were not readily observed (SI Figure S15), but the imaged cells had a higher concentration of phosphorus relative to that of imaged cells during periods of coagulant use (SI Figure S6). In either case (with or without coagulant addition), bulk liquid equilibrium modeling would not have predicted phosphorus precipitation; an accurate prediction of phosphorus distribution (including the formation of phosphorus- and metal-rich granules) would require more detailed analysis of the fate of organic and inorganic phosphorus in algae biomass to explicitly characterize mechanism of phosphorus accumulation, which is beyond the scope of this study.

The nitrogen content of solids was less variable than that of phosphorus. Across the focus period, the average biomass yield was 12.8 ± 0.7 kg TSS·(kg-N)$^{-1}$, corresponding to a solids nitrogen content of 7.8 ± 0.4% (average ± standard deviation; 5th/50th/95th percentiles of

7.10%/7.82%/8.49%). Similar to phosphorus, nitrogen content of microalgae can vary, with reported nitrogen content ranging from 5.87% to 11.16% of total solids.[48,49]

N:P mass ratios across the focus period were 2.5 ± 0.6 (SI Figure S16) but were notably higher prior to January 8, 2023 (3.3 ± 0.3, with phosphorus content of 2.4 ± 0.2%) than after (2.1 ± 0.2; with phosphorus content of 3.7 ± 0.4%). The nitrogen content remained relatively stable at 7.8 ± 0.5% to 7.9 ± 0.4% for the periods before and after January 8, 2023, respectively. Solids N:P ratio may vary with growth rate (linked to SRT) and influent N:P ratio through interspecific stoichiometric plasticity (especially under nutrient-limitation) or microbial community composition shifts in favor of species that have a competitive advantage in a given set of environmental conditions.[24,40,50] The relationship between influent N:P and solids N:P was not significant (linear $R^2 < 0.001$, n = 12), However, solids N:P had a negative linear correlation with SRT ($R^2 = 0.63$, SI Figure S17) during the period of superior performance (November 15, 2022 to February 14, 2023), varying from 2.1 to 4.2 days. In addition to SRT, the harvested solids N:P ratio of may also have been influenced by the fate of recovered phosphorus, which varied between assimilation within the cells and highly localized precipitation on the cell surfaces or within the EPS during upstream coagulant use.

3.1.3. Susceptibility to Process Upsets

Periods of process upset or variable performance were defined as periods of prolonged or intermittent exceedance of the 0.04 mg-P·L^{-1} effluent target, respectively. The system has been susceptible to process upsets driven by upstream changes to the wastewater treatment process (e.g., reduction in SBR settling time that resulted in TSS concentrations >100 mg-TSS·L^{-1} entering the EcoRecover process) and high influent concentrations of a disinfectant, quaternary ammonium. Periods of process upset or variable performance were often characterized by variable or basic pH, loss of DO diel rhythm, and at times included insufficient alkalinity and solids composition changes (details and images in SI Section S6 and Figure S18).

3.2. Carbon and Nutrient Dynamics across Unit Operations

Past work has demonstrated that carbohydrate storage and mobilization is important for the uptake of nutrients across light/dark cycles.[24,25] Specifically, exposure to lit, nutrient limited conditions can induce the storage of biopolymers which can then be leveraged under dark conditions to support nutrient uptake and continued metabolic activity. Thus, it was expected the storage and mobilization of carbohydrates may play a key role in the EcoRecover process. To better understand these dynamics, batch experiments were conducted on-site under mix tank (dark) and PBR (illuminated) conditions in May 2022 (prior examining the extant, full-scale carbon and nutrient dynamics) to characterize orthophosphate (**Figure 4**), ammonium (Figure S19), nitrate/nitrite (Figure S20), and biomass compositional (Figures S21, S22, S24-26) and concentration (Figure S23) trends. In the simulated mix tank (performed with simulated PBR culture mixed with EcoRecover influent), the initial orthophosphate of 0.337 ± 0.012 mg-P·L^{-1} was removed within 120 min (**Figure 4A**) and the initial ammonium concentration of 14 ± 2 mg-N·L^{-1} was reduced to 8.90 ± 0.01 mg-N·L^{-1} over the course of 240 min (Figure S19). In the simulated PBR (performed with EcoRecover mix tank effluent), the initial orthophosphate of 0.383 ± 0.015 mg-P·L^{-1} was removed within 40 min (**Figure 4A**) and the initial ammonium concentration of 36 ± 4 mg-N·L^{-1} was reduced to 5.24 ± 0.13 mg-N·L^{-1} over 360 min (Figure S19).

As expected, phosphorus limitation and the availability of light in the simulated PBR resulted in carbohydrate storage and an increase in the carbohydrate:protein ratio of solids and dark conditions in the simulated mix tank resulted in carbohydrate mobilization and a decrease in solids carbohydrate:protein ratio over time (**Figure 4B**). Consistent with this observation, the solids C:N and C:P mass ratios increased in the PBR and decreased in the mix tank across the bench-scale, batch experiments (SI Figures S21 and S22, respectively). PBR solids concentrations (quantified as VSS) increased from 470 ± 40 to 700 ± 20 mg·L^{-1} over 360 minutes, whereas mix tank VSS concentrations did not change significantly (two-sample t-test, two-tailed,

p = 0.876; SI Figure S23). Oxygen was produced under PBR conditions and consumed under mix tank conditions (SI Figure S24). No significant change in the solids N:P or lipids content was demonstrated over the course of the experiments (SI Figures S25 and S26, respectively). These bench-scale results confirmed that (i) photosynthesis in the PBRs supports the uptake of residual phosphorus, the accumulation carbohydrates in cell biomass, and the production of oxygen, and (ii) a significant amount of phosphorus removal occurs in dark, nutrient-rich conditions (i.e., the mix tank) and is facilitated by consumption of dissolved oxygen and the mobilization of stored carbohydrates.

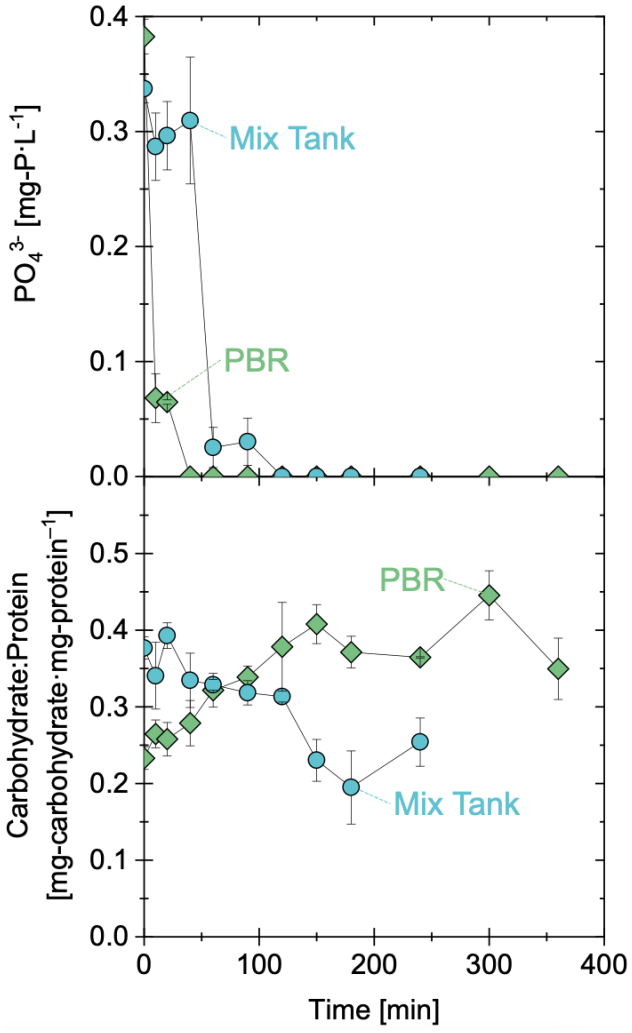

435

436 **Figure 4.** (A) Orthophosphate and (B) carbohydrate:protein ratios in bench-scale batch
437 experiments to mimic conditions in the mix tank (blue circles) and PBRs (green diamonds).
438 Batch experiments were run in duplicate. The duration of the experiments was at least twice the
439 HRT of the full-scale unit processes. Mix tank experiments were carried out with bench-scale
440 PBR culture combined with full-scale secondary effluent. PBR experiments were carried out with
441 full-scale mix tank culture. Symbols represent averages, error bars extending to individual
442 replicate (i.e., minimum and maximum) values.

443

In the full-scale system, similar trends were observed with higher biomass C:N ratios (and carbohydrate:protein ratios) in the PBR effluent than the mix tank effluent during periods of good performance (**Figure 5**, SI Figure S27). The consistency of higher C:N ratios in biomass leaving the PBRs relative to the biomass leaving the mix tank further underscores the importance of stored carbohydrates in nutrient recovery. To further elucidate the relationship between carbohydrate dynamics and nutrient recovery, the mobilized carbohydrates (consumed in the dark environment of the mix tank) were normalized to the quantity of phosphorus recovered from the system. Across the full focus period, the average amount of carbohydrate mobilized per phosphorus recovered was 19 g-carbohydrate·g-P^{-1} (n = 30), which was approximately half the value in past bench-scale P-limited experiments.[24] Although orthophosphate was measured online in the system influent and effluent, it was not measured in the mix tank effluent; therefore, the carbohydrate and C:N dynamics relative to phosphorus uptake could not be quantified, and may be a focus of future work to continue to inform the design and optimization of the EcoRecover process. Overall, the storage and mobilization of carbohydrates enabled continuous nutrient removal in the mix tank with residual polishing in the PBRs.

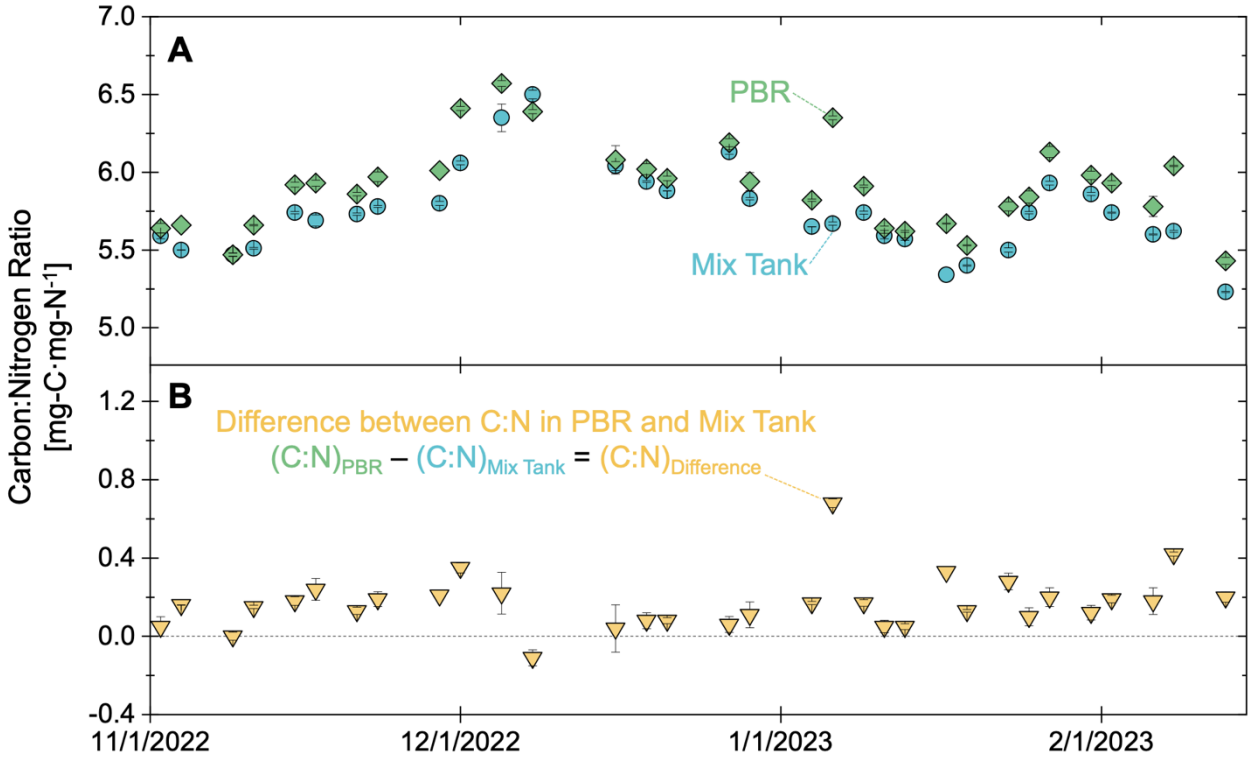

Figure 5. (A) Solids C:N ratio (by mass) in the full-scale mix tank (blue circles) and PBR (green diamonds) effluent from November 1, 2022 to February 14, 2023. Error bars represent relative error from analytical duplicates. (B) Difference between the PBR and mix tank solids C:N ratios, with positive values supporting the hypothesis that the microbial community was storing carbohydrates in the PBRs and mobilizing (i.e., consuming) stored carbohydrates in the mix tank. Error bars in (B) represent propagated relative error (SI Equation S1) from analytical duplicates in (A).

3.3. A Path Forward for Intensive, Suspended Growth, Mixed Microalgal Wastewater Treatment

Wastewater resource recovery facilities that support urban populations are often landlocked and need to intensify their processes to meet more stringent effluent permits or increase their treatment capacity.[51] Adoption of high productivity, small footprint (intensive) microalgal

technologies creates an opportunity to sustainably convert waste nutrients to marketable products and meet rigorous effluent nutrient criteria. While enhanced biological phosphorus removal (EBPR) may remove phosphorus to effluent concentrations approaching 0.1 mg-P·L^{-1}, the EcoRecover process has demonstrated long-term recovery of phosphorus to achieve effluent total phosphorus concentrations below 0.03 mg-P·L^{-1}, even in winter months in Wisconsin (latitude of 45° N). An additional advantage of algal-based systems is the potential for organic phosphorus (and organic nitrogen) recovery,[11] which remain a critical challenge for conventional bacterial and precipitation-based nutrient removal technologies.[52] Future studies may specifically focus on organic nutrient recovery, as well as the sustainability implications (e.g., reduced chemical dosages and CO_2 sequestration)[53] of replacing alternative tertiary treatment processes such as chemical phosphorus polishing.

In the algal cultivation space, technologies are often compared based on their areal productivities. In this study, the characterized EcoRecover process was intentionally designed to be phosphorus-limited to meet stringent permit requirements. As a result, the system was not designed to maximize biomass productivity and instead prioritized reliable effluent quality (with biomass production and sale serving as a secondary benefit). Nonetheless, across the focus period (November 1, 2022 to February 14, 2023), the EcoRecover's areal productivity was 15 ± 4 g·m^{-2}·day^{-1} in winter months (external temperatures from -27 to 24 °C, daily average of -7 °C) at a high altitude (45° N). In other monitored periods subject to upstream upsets or other external pressures (e.g., chemical shortages), areal productivities on the order of 45 g·m^{-2}·d^{-1} (average from July 26 to September 6, 2022; individual timepoint estimates ranged from 36 to 60 g·m^{-2}·d^{-1}) were also observed.

Ultimately, this work represents the first full-scale characterization of the EcoRecover process for algae cultivation and tertiary nutrient recovery. Parallel studies will include more in-depth analyses of the microbial ecology, including longer-term sequencing results and more in-

depth community structure analyses.[54] Future work will continue to build off this understanding to advance our ability to optimize the design of this system, mechanistically and dynamically model its performance, and develop tailored solutions for utilities seeking to simultaneously advance goals for improved effluent quality and engagement with the circular bioeconomy.

Acknowledgements

The authors would like to acknowledge the Village of Roberts Director of Public Works, John Bond, and the Public Works staff for their on-site support and expertise; Elizabeth Eves and Dr. Ashley Blystone of the University of Illinois Urbana-Champaign Microanalysis Laboratory for elemental analysis of many biomass samples; Samuel Aguiar for ion chromatography training and trouble-shooting; Jorge Corral for sample processing and data compilation; and the UIUC Environmental Engineering and Science Laboratory Manager, Dr. Shaoying Qi, for laboratory support. This material is based upon work supported by the U.S. Department of Energy, Office of Energy Efficiency and Renewable Energy, under Award Number DE-EE0009270.

Supplemental Information Available

The following Supporting Information is available:

Images of the EcoRecover system at Roberts, WI, USA; Detailed descriptions of on-line monitoring equipment; Expanded continuous monitoring results for system performance; Detailed description of ion chromatography analyses; Descriptions of periods of system performance upset; Solids characterization through SEM-EDS; Batch experiment aqueous and biomass analyses. (PDF)

Cleaned long-term AIMS monitoring data from November 1, 2022 through February 14, 2023 (XLSX)

Cleaned long-term SCADA monitoring data from November 1, 2022 through February 14, 2023 (XLSX)

Author information

Corresponding Author

Jeremy S. Guest - Institute for Sustainability, Energy, and Environment, University of Illinois at Urbana-Champaign, 1101 West Peabody Drive, Urbana, Illinois 61801, United States; Department of Civil and Environmental Engineering, University of Illinois at Urbana-Champaign, 205 North Mathews Avenue, Urbana, Illinois 61801, United States; Orcid https://orcid.org/0000-0003-2489-2579

Authors

Hannah R. Molitor – Department of Civil and Environmental Engineering, University of Illinois at Urbana-Champaign, 205 North Mathews Avenue, Urbana, Illinois 61801, United States; Orcid http://orcid.org/0000-0003-4855-5358

Ga-Yeong Kim - Department of Civil and Environmental Engineering, University of Illinois at Urbana-Champaign, 205 North Mathews Avenue, Urbana, Illinois 61801, United States; Orcid https://orcid.org/0000-0002-9664-1923

Elaine Hartnett - Clearas Water Recovery, Inc., 1500 Clark Fork Ln, Missoula, Montana 59808, United States

Benjamin Gincley - School of Civil and Environmental Engineering, Georgia Institute of Technology, Atlanta, Georgia 30332, United States; Orcid https://orcid.org/0000-0001-8824-7144

Mahbub Alam – Department of Civil, Structural and Environmental Engineering, University at Buffalo, 212 Ketter Hall, Buffalo, New York 14260, United States; Orcid https://orcid.org/0000-0003-1984-3190

Nickolas M. Avila - Department of Civil and Environmental Engineering, University of Illinois at Urbana-Champaign, 205 North Mathews Avenue, Urbana, Illinois 61801, United States

Jianan Feng – Department of Civil and Environmental Engineering, University of Illinois at Urbana-Champaign, 205 North Mathews Avenue, Urbana, Illinois 61801, United States; Orcid https://orcid.org/0000-0001-6987-1187

Autumn Fisher - Clearas Water Recovery, Inc., 1500 Clark Fork Ln, Missoula, Montana 59808, United States

Mahdi Hodaei – Department of Civil, Structural and Environmental Engineering, University at Buffalo, 212 Ketter Hall, Buffalo, New York 14260, United States; Orcid https://orcid.org/0000-0001-7781-0093

Yalin Li* - Institute for Sustainability, Energy, and Environment, University of Illinois at Urbana-Champaign, 1101 West Peabody Drive, Urbana, Illinois 61801, United States; Orcid https://orcid.org/0000-0002-8863-4758

*Current address: Department of Civil and Environmental Engineering, Rutgers, The State University of New Jersey, 500 Bartholomew Road, Piscataway, NJ 08854, United States

Kevin McGraw - Clearas Water Recovery, Inc., 1500 Clark Fork Ln, Missoula, Montana 59808, United States

Roland D. Cusick – Department of Civil and Environmental Engineering, University of Illinois at Urbana-Champaign, 205 North Mathews Avenue, Urbana, Illinois 61801, United States; Orcid https://orcid.org/0000-0002-4037-2939

Ian M. Bradley - Department of Civil, Structural and Environmental Engineering, University at Buffalo, 212 Ketter Hall, Buffalo, New York 14260, United States; Research and Education in Energy, Environment and Water Institute, University at Buffalo, 112 Cooke Hall, Buffalo, New York 14260, United States; Orcid https://orcid.org/0000-0001-5338-1167

Ameet J. Pinto - School of Civil and Environmental Engineering, Georgia Institute of Technology, Atlanta, Georgia 30332, United States; Orcid https://orcid.org/0000-0003-1089-5664

References

(1) Nutrients Working Group. *Nutrient Redution Progress Tracker Version 1.0- 2017*; Association of Clean Water Administrators, 2018. https://www.acwa-us.org/wp-content/uploads/2018/03/Nutrient-Reduction-Progress-Tracker-Version-1.0-2017-Report.pdf (accessed 2022-07-19).

(2) Schindler, D. W.; Carpenter, S. R.; Chapra, S. C.; Hecky, R. E.; Orihel, D. M. Reducing Phosphorus to Curb Lake Eutrophication Is a Success. *Environ. Sci. Technol.* **2016**, *50* (17), 8923–8929. https://doi.org/10.1021/acs.est.6b02204.

(3) US EPA. *Progress towards Adopting Total Nitrogen and Total Phosphorus Numeric Water Quality Standards*. US EPA Nutrient Policy and Data. https://www.epa.gov/nutrient-policy-data/progress-towards-adopting-total-nitrogen-and-total-phosphorus-numeric-water (accessed 2022-07-19).

(4) US EPA. *N/P Criteria Progress Map*. State Progress Toward Developing Numeric Nutrient Water Quality Criteria for Nitrogen and Phosphorus. https://www.epa.gov/nutrient-policy-data/state-progress-toward-developing-numeric-nutrient-water-quality-criteria#tb3 (accessed 2022-07-20).

(5) Li, X.; Shen, S.; Xu, Y.; Guo, T.; Dai, H.; Lu, X. Application of Membrane Separation Processes in Phosphorus Recovery: A Review. *Science of The Total Environment* **2021**, *767*, 144346. https://doi.org/10.1016/j.scitotenv.2020.144346.

(6) Bunce, J. T.; Ndam, E.; Ofiteru, I. D.; Moore, A.; Graham, D. W. A Review of Phosphorus Removal Technologies and Their Applicability to Small-Scale Domestic Wastewater Treatment Systems. *Frontiers in Environmental Science* **2018**, *6*.

(7) Zahed, M. A.; Salehi, S.; Tabari, Y.; Farraji, H.; Ataei-Kachooei, S.; Zinatizadeh, A. A.; Kamali, N.; Mahjouri, M. Phosphorus Removal and Recovery: State of the Science and Challenges. *Environ Sci Pollut Res* **2022**, *29* (39), 58561–58589. https://doi.org/10.1007/s11356-022-21637-5.

(8) Bott, C. B.; Parker, D. S. *Nutrient Management Volume II: Removal Technology Performance & Reliability*; Water Environment Research Foundation: Alexandria, VA, 2011. https://www.waterrf.org/resource/nutrient-management-volume-ii-removal-technology-performance-reliability.

(9) HydroQual, Inc.; Stensel, D. H. *Wastewater Phosphorus Control and Reduction Initiative*; Prepared for the Minnesota Environmental Science and Economic Review Board.; 2005; pp 37–38. https://wrl.mnpals.net/islandora/object/WRLrepository%3A941/datastream/PDF/view (accessed 2022-11-07).

(10) Petzet, S.; Peplinski, B.; Bodkhe, S. Y.; Cornel, P. Recovery of Phosphorus and Aluminium from Sewage Sludge Ash by a New Wet Chemical Elution Process (SESAL-Phos-Recovery Process). *Water Science and Technology* **2011**, *64* (3), 693–699. https://doi.org/10.2166/wst.2011.682.

(11) Qin, C.; Liu, H.; Liu, L.; Smith, S.; Sedlak, D. L.; Gu, A. Z. Bioavailability and Characterization of Dissolved Organic Nitrogen and Dissolved Organic Phosphorus in Wastewater Effluents. *Science of The Total Environment* **2015**, *511*, 47–53. https://doi.org/10.1016/j.scitotenv.2014.11.005.

(12) Sutherland, D. L.; Bramucci, A. Dissolved Organic Phosphorus Bioremediation from Food-Waste Centrate Using Microalgae. *Journal of Environmental Management* **2022**, *313*, 115018. https://doi.org/10.1016/j.jenvman.2022.115018.

(13) Mayer, B. K.; Baker, L. A.; Boyer, T. H.; Drechsel, P.; Gifford, M.; Hanjra, M. A.; Parameswaran, P.; Stoltzfus, J.; Westerhoff, P.; Rittmann, B. E. Total Value of Phosphorus Recovery. *Environ. Sci. Technol.* **2016**, *50* (13), 6606–6620. https://doi.org/10.1021/acs.est.6b01239.

(14) *Clearas Water Recovery, Inc.* https://www.clearassolutions.com/ (accessed 2022-07-15).

(15) *Village of Roberts, Wisconsin*. https://www.robertswisconsin.com/ (accessed 2022-07-14).

(16) Wisconsin Department of Natural Resources. *2022 Water Conditions: List Appendix A-Impaired Waters List*. Water Conditions Lists. https://dnr.wisconsin.gov/topic/SurfaceWater/ConditionLists.html (accessed 2022-07-26).

(17) Rieger, L. Guidelines for Using Activated Sludge Models. *wio* **2012**, *11*. https://doi.org/10.2166/9781780401164.
(18) *KernelSmoother*. scikit-fda. https://fda.readthedocs.io/en/stable/modules/preprocessing/autosummary/skfda.preprocessing.smoothing.KernelSmoother.html (accessed 2023-11-13).
(19) Kim, G.-Y.; Molitor, H. R.; Zhang, X.; Li, Y.; Avila, N. M.; Shoener, B. D.; Schramm, S. M.; Morgenroth, E.; Snowling, S. D.; Bradley, I. M.; Pinto, A. J.; Guest, J. S. Development and Validation of a Phototrophic-Mixotrophic Process Model (PM2) and a Process Simulator for Microalgae-Based Wastewater Treatment. https://doi.org/In preparation.
(20) Ripp, J. *Analytical Detection Limit Guidance & Laboratory Guide for Determining Method Detection Limits*; Wisconsin Department of Natural Resources, Laboratory Certification Program, 1996.
(21) Pruvost, J.; Van Vooren, G.; Cogne, G.; Legrand, J. Investigation of Biomass and Lipids Production with Neochloris Oleoabundans in Photobioreactor. *Bioresource Technology* **2009**, *100* (23), 5988–5995. https://doi.org/10.1016/j.biortech.2009.06.004.
(22) Lourenço, S. O.; Barbarino, E.; Marquez, U. M. L.; Aidar, E. Distribution of Intracellular Nitrogen in Marine Microalgae: Basis for the Calculation of Specific Nitrogen-to-protein Conversion Factors. *Journal of Phycology* **1998**, *34* (5), 798–811. https://doi.org/10.1046/j.1529-8817.1998.340798.x.
(23) Van Wychen, S.; Laurens, L. M. L. *Determination of Total Carbohydrates in Algal Biomass: Laboratory Analytical Procedure*; Technical Report NREL/TP-5100-60957; National Renewable Energy Laboratory: Golden, CO, 2015.
(24) Gardner-Dale, D. A.; Bradley, I. M.; Guest, J. S. Influence of Solids Residence Time and Carbon Storage on Nitrogen and Phosphorus Recovery by Microalgae across Diel Cycles. *Water Research* **2017**, *121*, 231–239. https://doi.org/10.1016/j.watres.2017.05.033.
(25) Bradley, I. M.; Li, Y.; Guest, J. S. Solids Residence Time Impacts Carbon Dynamics and Bioenergy Feedstock Potential in Phototrophic Wastewater Treatment Systems. *Environ. Sci. Technol.* **2021**. https://doi.org/10.1021/acs.est.1c02590.
(26) Mañas, A.; Biscans, B.; Spérandio, M. Biologically Induced Phosphorus Precipitation in Aerobic Granular Sludge Process. *Water Research* **2011**, *45* (12), 3776–3786. https://doi.org/10.1016/j.watres.2011.04.031.
(27) Liu, Y.-Q.; Cinquepalmi, S. Exploration of Mechanisms for Calcium Phosphate Precipitation and Accumulation in Nitrifying Granules by Investigating the Size Effects of

664 Granules. *Water Research* **2021**, *206*, 117753.
665 https://doi.org/10.1016/j.watres.2021.117753.
666 (28) Huang, W.; Huang, W.; Li, H.; Lei, Z.; Zhang, Z.; Tay, J. H.; Lee, D.-J. Species and
667 Distribution of Inorganic and Organic Phosphorus in Enhanced Phosphorus Removal
668 Aerobic Granular Sludge. *Bioresource Technology* **2015**, *193*, 549–552.
669 https://doi.org/10.1016/j.biortech.2015.06.120.
670 (29) Axelsson, M.; Gentili, F. A Single-Step Method for Rapid Extraction of Total Lipids from
671 Green Microalgae. *PLoS One* **2014**, *9* (2), e89643.
672 https://doi.org/10.1371/journal.pone.0089643.
673 (30) Folch, J.; Lees, M.; Sloane Stanley, G. H. A Simple Method for the Isolation and
674 Purification of Total Lipides from Animal Tissues. *J. Biol. Chem.* **1957**, *226* (1), 497–509.
675 (31) Bradley, I. M.; Pinto, A. J.; Guest, J. S. Design and Evaluation of Illumina MiSeq-
676 Compatible, 18S rRNA Gene-Specific Primers for Improved Characterization of Mixed
677 Phototrophic Communities. *Appl. Environ. Microbiol.* **2016**, *82* (19), 5878–5891.
678 https://doi.org/10.1128/AEM.01630-16.
679 (32) Kozich, J. J.; Westcott, S. L.; Baxter, N. T.; Highlander, S. K.; Schloss, P. D.
680 Development of a Dual-Index Sequencing Strategy and Curation Pipeline for Analyzing
681 Amplicon Sequence Data on the MiSeq Illumina Sequencing Platform. *Appl. Environ.*
682 *Microbiol.* **2013**, AEM.01043-13. https://doi.org/10.1128/AEM.01043-13.
683 (33) Excoffier, L.; Smouse, P. E.; Quattro, J. M. Analysis of Molecular Variance Inferred from
684 Metric Distances among DNA Haplotypes: Application to Human Mitochondrial DNA
685 Restriction Data. *Genetics*, 1992, *131*, 479–491.
686 (34) Garcia, N. S.; Sexton, J.; Riggins, T.; Brown, J.; Lomas, M. W.; Martiny, A. C. High
687 Variability in Cellular Stoichiometry of Carbon, Nitrogen, and Phosphorus Within Classes of
688 Marine Eukaryotic Phytoplankton Under Sufficient Nutrient Conditions. *Front. Microbiol.*
689 **2018**, *9*, 543. https://doi.org/10.3389/fmicb.2018.00543.
690 (35) Finkel, Z. V.; Follows, M. J.; Liefer, J. D.; Brown, C. M.; Benner, I.; Irwin, A. J.
691 Phylogenetic Diversity in the Macromolecular Composition of Microalgae. *PLoS ONE* **2016**,
692 *11* (5), e0155977. https://doi.org/10.1371/journal.pone.0155977.
693 (36) Choi, H. J.; Lee, S. M. Effect of the N/P Ratio on Biomass Productivity and Nutrient
694 Removal from Municipal Wastewater. *Bioprocess Biosyst Eng* **2015**, *38* (4), 761–766.
695 https://doi.org/10.1007/s00449-014-1317-z.

(37) Beuckels, A.; Smolders, E.; Muylaert, K. Nitrogen Availability Influences Phosphorus Removal in Microalgae-Based Wastewater Treatment. *Water Research* **2015**, *77*, 98–106. https://doi.org/10.1016/j.watres.2015.03.018.

(38) Rhee, G.-Y. A Continuous Culuture Study of Phosphate Uptake, Growth Rate and Polyphosphate in *Scenedesmus* Sp. [1]. *Journal of Phycology* **1973**, *9* (4), 495–506. https://doi.org/10.1111/j.1529-8817.1973.tb04126.x.

(39) Whitton, R.; Le Mével, A.; Pidou, M.; Ometto, F.; Villa, R.; Jefferson, B. Influence of Microalgal N and P Composition on Wastewater Nutrient Remediation. *Water Research* **2016**, *91*, 371–378. https://doi.org/10.1016/j.watres.2015.12.054.

(40) Geider, R.; La Roche, J. Redfield Revisited: Variability of C:N:P in Marine Microalgae and Its Biochemical Basis. *European Journal of Phycology* **2002**, *37* (1), 1–17. https://doi.org/10.1017/S0967026201003456.

(41) Grobbelaar, J. U. Inorganic Algal Nutrition. *Handbook of microalgal culture: applied phycology and biotechnology* **2013**, 123–133.

(42) Solovchenko, A. E.; Ismagulova, T. T.; Lukyanov, A. A.; Vasilieva, S. G.; Konyukhov, I. V.; Pogosyan, S. I.; Lobakova, E. S.; Gorelova, O. A. Luxury Phosphorus Uptake in Microalgae. *Journal of Applied Phycology* **2019**, *31* (5), 2755–2770. https://doi.org/10.1007/s10811-019-01831-8.

(43) Powell, N.; Shilton, A. N.; Pratt, S.; Chisti, Y. Factors Influencing Luxury Uptake of Phosphorus by Microalgae in Waste Stabilization Ponds. *Environ. Sci. Technol.* **2008**, *42* (16), 5958–5962. https://doi.org/10.1021/es703118s.

(44) Sanz-Luque, E.; Bhaya, D.; Grossman, A. R. Polyphosphate: A Multifunctional Metabolite in Cyanobacteria and Algae. *Front. Plant Sci.* **2020**, *11*, 938. https://doi.org/10.3389/fpls.2020.00938.

(45) Zerveas, S.; Mente, M. S.; Tsakiri, D.; Kotzabasis, K. Microalgal Photosynthesis Induces Alkalization of Aquatic Environment as a Result of H+ Uptake Independently from CO2 Concentration – New Perspectives for Environmental Applications. *Journal of Environmental Management* **2021**, *289*, 112546. https://doi.org/10.1016/j.jenvman.2021.112546.

(46) Hartley, A. M.; House, W. A.; Callow, M. E.; Leadbeater, B. S. C. Coprecipitation of Phosphate with Calcite in the Presence of Photosynthesizing Green Algae. *Water Research* **1997**, *31* (9), 2261–2268. https://doi.org/10.1016/S0043-1354(97)00103-6.

(47) Xu, M.; Bernards, M.; Hu, Z. Algae-Facilitated Chemical Phosphorus Removal during High-Density Chlorella Emersonii Cultivation in a Membrane Bioreactor. *Bioresource Technology* **2014**, *153*, 383–387. https://doi.org/10.1016/j.biortech.2013.12.026.

(48) Tibbetts, S. M.; Milley, J. E.; Lall, S. P. Chemical Composition and Nutritional Properties of Freshwater and Marine Microalgal Biomass Cultured in Photobioreactors. *J Appl Phycol* **2015**, *27* (3), 1109–1119. https://doi.org/10.1007/s10811-014-0428-x.

(49) Molitor, H. R.; Schnoor, J. L. Using Simulated Flue Gas to Rapidly Grow Nutritious Microalgae with Enhanced Settleability. *ACS Omega* **2020**, *5* (42), 27269–27277. https://doi.org/10.1021/acsomega.0c03492.

(50) Valverde-Pérez, B.; Ramin, E.; Smets, B. F.; Plósz, B. G. EBP2R – An Innovative Enhanced Biological Nutrient Recovery Activated Sludge System to Produce Growth Medium for Green Microalgae Cultivation. *Water Research* **2015**, *68*, 821–830. https://doi.org/10.1016/j.watres.2014.09.027.

(51) Sturm, B. *State of Knowledge and Workshop Report: Intensification of Resource Recovery (IR2) Forum*; TIRR1R15; Water Environment Research Foundation: Alexandria, VA, 2016.

(52) Clark, D. L. Nutrient Management: Regulatory Approaches to Protect Water Quality: Volume 1 – Review of Existing Practices. *wio* **2010**, *9*. https://doi.org/10.2166/9781780403465.

(53) Falk, M. W.; Reardon, D. J.; Neethling, J. B.; Clark, D. L.; Pramanik, A. Striking the Balance between Nutrient Removal, Greenhouse Gas Emissions, Receiving Water Quality, and Costs. *Water Environment Research* **2013**, *85* (12), 2307–2316. https://doi.org/10.2175/106143013X13807328848379.

(54) Alam, M. M.; Hodaei, M.; Hartnett, E.; Gincley, B.; Kim, G.-Y.; Pinto, A. J.; Bradley, I. M. Community Structure and Function During Periods of High Performance and System Upset in a Full-Scale Mixed Microalgal Wastewater Resource Recovery Facility. **In preparation**.